

A 193 nm laser photofragmentation timeofflight mass spectrometric study of CS₂ and CS₂ clusters

W.B. Tzeng, H.M. Yin, W.Y. Leung, J.Y. Luo, S. Nourbakhsh, G. D. Fleisch, and C. Y. Ng

Citation: *The Journal of Chemical Physics* **88**, 1658 (1988); doi: 10.1063/1.454144

View online: <http://dx.doi.org/10.1063/1.454144>

View Table of Contents: <http://scitation.aip.org/content/aip/journal/jcp/88/3?ver=pdfcov>

Published by the [AIP Publishing](#)

Articles you may be interested in

[A laser photofragmentation time-of-flight mass spectrometric study of acetophenone at 193 and 248 nm](#)
J. Chem. Phys. **107**, 7230 (1997); 10.1063/1.474964

[A 193-nm-laser photofragmentation time-of-flight mass spectrometric study of dimethylsulfoxide](#)
J. Chem. Phys. **106**, 86 (1997); 10.1063/1.473025

[Statespecific neutral timeofflight of CO from ketene photodissociation at 351 nm: The internal energy distribution of CH₂\(\$\tilde{X}^3 B_1\$ \)](#)
J. Chem. Phys. **105**, 4550 (1996); 10.1063/1.472538

[193 nm laser photofragmentation timeofflight mass spectrometric study of HSCH₂CH₂SH](#)
J. Chem. Phys. **104**, 130 (1996); 10.1063/1.470883

[A 193 nm laser photofragmentation timeofflight mass spectrometric study of CH₃SSCH₃, SSCH₃, and SCH₃](#)
J. Chem. Phys. **92**, 6587 (1990); 10.1063/1.458295



A 193 nm laser photofragmentation time-of-flight mass spectrometric study of CS₂ and CS₂ clusters

W.-B. Tzeng,^{a)} H.-M. Yin,^{b)} W.-Y. Leung, J.-Y. Luo,^{b)} S. Nourbakhsh, G. D. Flesch, and C. Y. Ng^{c)}

Ames Laboratory,^{d)} U. S. Department of Energy and Department of Chemistry, Iowa State University, Ames, Iowa 50011

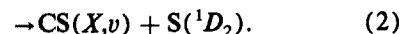
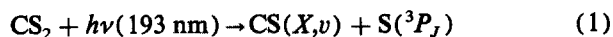
(Received 23 September 1987; accepted 15 October 1987)

A crossed laser and molecular beam photofragmentation apparatus is described. The apparatus is equipped with a rotatable molecular beam source and a translationally movable ultrahigh vacuum mass spectrometer for time-of-flight (TOF) measurements. Using this apparatus we have measured the TOF spectra of S and CS resulting from the photofragmentation processes, $\text{CS}_2 + h\nu(193 \text{ nm}) \rightarrow \text{CS}(X,v) + \text{S}(^1D \text{ or } ^3P)$. The translational energy distributions of photofragments derived from the S and CS TOF spectra are in good agreement. This observation, together with the finding that the TOF spectra of S and CS are independent of laser power in the 25–150 mJ range, shows that the further absorption of a laser photon by CS to form $\text{C}(^3P) + \text{S}(^3P)$ within the laser pulse is insignificant. The TOF spectra of S obtained at electron ionization energies of 20 and 50 eV are indiscernible, indicating that the contribution to the TOF spectrum of S from dissociative ionization of CS is negligible at electron impact energies <50 eV. The thermochemical thresholds for the S(¹D) and S(³P) channels are determined to be 18.7 and 45.0 ± 0.4 kcal/mol, respectively, consistent with literature values. Structures found in the translational energy distribution can be correlated with vibrational structures of CS($X,v=0-5$) associated with the S(¹D) channel. The translational energy distribution supports the previous observation that the vibrational state distribution of CS(X,v) is peaked at $v=3$. The TOF experiment is also consistent with the S(³P)/S(¹D) ratio of 2.8 ± 0.3 determined in a recent vacuum ultraviolet laser induced fluorescence measurement on the S photofragment. Photofragments from CS₂ clusters are observed at small laboratory angles with respect to the CS₂ beam direction and are found to have velocity distributions peaked at the CS₂ cluster beam velocity.

I. INTRODUCTION

Photodissociation studies of triatomic molecules have been a rich and mature subfield in photofragment dynamics.¹⁻⁶ Due to the advances in laser technology, spectroscopic techniques, and molecular beams, the photodissociation studies of many triatomic molecules have been performed to the detail of state-to-state levels. The precise experimental data obtained have allowed direct comparisons with rigorous theoretical predictions. The satisfactory agreement between experimental and theoretical results for photofragment dynamics of diatomic and triatomic molecules is an important step for further understanding of photodissociation processes involving polyatomic molecules.

Although the photochemistry of CS₂ in the wavelength region of 180–210 nm has been investigated by various spectroscopic techniques,⁷⁻²² detailed agreement between these experiments is lacking. The most controversial result is the branching ratio for the S(³P) and S(¹D) channels formed by the photodissociation of CS₂ at 193 nm:



The ratio for S(³P)/S(¹D) obtained previously varies by more than an order of magnitude. The problem in determining the vibrational distribution of CS(X,v) by the laser induced fluorescence method is the strong absorption of CS(X,v) at 193 nm within the dissociating laser pulse resulting in the $A-X$ transition. The subsequent emission of CS(A,v') to CS(X,v) makes the laser induced fluorescence experiment difficult. The absorption of a 193 nm excimer laser photon by CS($X,v>5$) may also induce the decomposition of CS($X,v>5$) to give S(³P) and C(³P).¹⁶ If the latter process occurs, the result of the branching ratio measurement will be erroneous. Furthermore, the efficient quenching of S(¹D) by CS₂ may affect the measured branching ratio if S(¹D) and S(³P) are not monitored at a sufficiently short delay time after the excimer laser pulse.

The most recent photodissociation studies²⁰⁻²² of CS₂ at 193 nm have added to the controversy concerning the S(³P)/S(¹D) branching ratio. By examining the time-resolved vibration-rotation spectral lines of CS(X,v,J), Kanamori and Hirota²¹ estimated the branching ratio as 1. A value of 0.66 for S(³P)/S(¹D) was obtained by McCrary *et al.*²⁰ based on the time-of-flight (TOF) spectrum for CS measured at 0° laboratory angle with respect to the CS₂ beam direction and laser induced fluorescence measurements of

^{a)} Present address: Department of Chemistry, Pennsylvania State University.

^{b)} Visiting Scholar, Dalian Institute of Chemical Physics, Dalian, Peoples Republic of China.

^{c)} Camille and Henry Dreyfus Teacher-Scholar.

^{d)} Operated for the U. S. Department of Energy by Iowa State University under Contract No. W-7405-Eng-82. This work was supported by the Director of Energy Research, Office of Basic Energy Sciences.

CS. The laser induced fluorescence detection of S(³P) and S(¹D) using a vacuum ultraviolet (VUV) laser by Waller *et al.*²² gives a value of 2.8 for the S(³P)/S(¹D) ratio.

The previous experimental results are consistent with the conclusion that the vibrational population of the CS fragment is peaked at $v \approx 3$. This conclusion is not confirmed by the infrared laser kinetic spectroscopic study of Kanamori and Hirota.²¹

Since the pioneering work of Wilson and co-workers,^{23–27} the crossed laser and molecular beam photofragmentation spectroscopy with TOF mass spectrometric detection was established to be a universal and detailed method of investigating photodissociation dynamics. Two TOF mass spectrometric experiments have been performed on 193 nm photodissociation of CS₂. The earlier experiment of Yang *et al.*¹⁸ measured the TOF spectrum of CS at 90° laboratory angle with respect to the CS₂ beam direction. Therefore, CS fragments having center-of-mass (c.m.) velocities lower than the CS₂ beam velocity are not detected. The translational energy distribution derived from the 90° TOF spectrum of CS is peaked at ~ 5 kcal/mol. However, the more recent measurement of the TOF spectrum of CS at 0° laboratory angle gives a translational energy distribution which is nearly a monotonically decreasing function of translational energy. The greatest population of photofragments are found to be near thermal energy.

In order to shed light on the different results of the previous TOF experiments, we have performed a 193 nm laser photofragment TOF mass spectrometric experiment on CS₂ using a newly constructed rotating beam source laser photofragmentation apparatus in our laboratory. A similar rotating beam source laser photofragmentation apparatus has been reported recently.²⁸ The unique feature of our appara-

tus is the translationally movable mass spectrometer which allows the flight path (L) to be varied. At a high signal level, a long flight path can be used to achieve high resolution in TOF measurements. In this study, the TOF spectra for both CS and S are measured. The effects of ionization electron energy and laser power on the measured TOF spectra are examined. Time-of-flight spectra of photofragments from CS₂ clusters are also presented in this report.

II. EXPERIMENTAL

The cross section of the rotatable beam source laser photofragmentation apparatus is shown in Fig. 1. The apparatus can be divided into three main components: an ArF excimer laser, a photodissociation chamber in which a rotatable supersonic molecular beam intersects with the laser beam, and a linearly movable ultrahigh vacuum electron ionization mass spectrometric detector.

A pure CS₂ beam or a beam of CS₂ seeded in He(Ne) is produced by supersonic expansion through a stainless nozzle (1) with a diameter of 0.127 mm. The nozzle stagnation partial pressure of CS₂ is kept constant at ~ 150 Torr, the vapor pressure of CS₂ at 0 °C, by placing CS₂ in a stainless-steel container submerged in a water-ice bath. The seeded CS₂ beam is formed by bubbling the He(Ne) carrier gas through liquid CS₂ before allowing the mixture of CS₂ vapor and He(Ne) to expand through the nozzle. The molecular beam source is pumped by a 20 in. diffusion pump (DP) (Varian HS20) with a pumping speed of $\sim 20\,000$ ℓ/s . At a nozzle stagnation pressure (P_0) of 15 psi for the CS₂/He seed beam, a pressure of $\lesssim 1 \times 10^{-4}$ Torr is maintained in the beam source chamber. The CS₂ beam has an angular divergence of 3° which is defined by the opening of a conical skimmer and a circular aperture as it passes through the

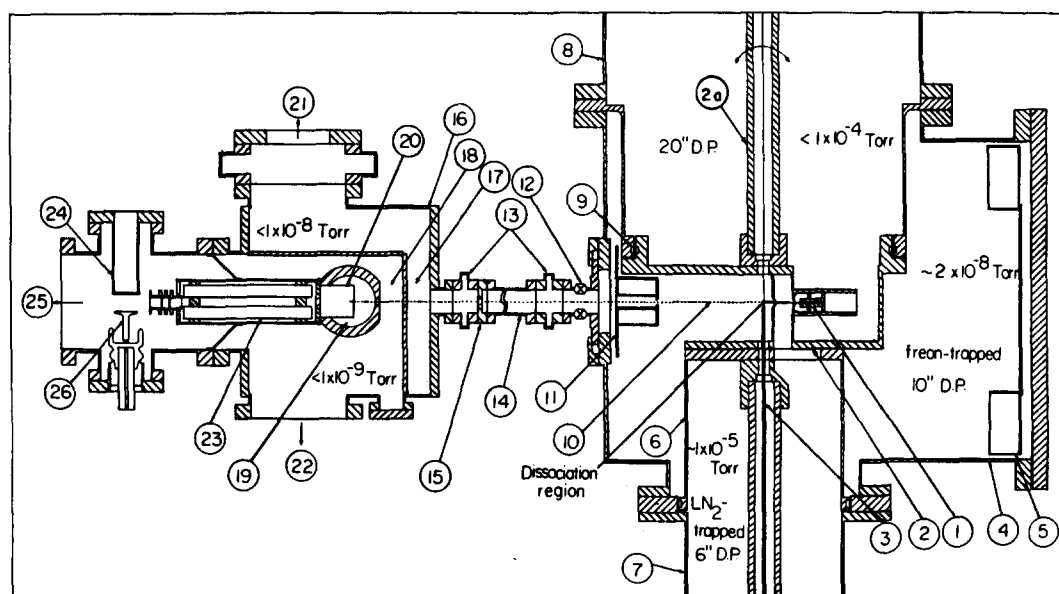


FIG. 1. Cross-sectional view of the rotating beam source photofragmentation apparatus. (1) nozzle, (2) rotatable molecular beam source chamber, (2a) shaft, (3) excimer laser beam, (4) photodissociation chamber, (5) liquid-nitrogen-cooled cold trap, (6) rotatable differential pumping chamber, (7) differential pumping chamber, (8) molecular beam source chamber, (9) bearing, (10) detector axis, (11) liquid-nitrogen cold trap, (12) flexible bellow, (13) valve, (14) extension tube, (15) adjustable aperture, (16) detector chamber, (17) first differential pumping region, (18) second differential pumping region, (19) ionization region, (20) ionizer, (21) turbomolecular pump (Balzer TPU310), (22) ion pump (Ultek DI pump, 220 ℓ/s), (23) quadrupole mass filter, (24) photomultiplier assembly, (25) liquid-nitrogen trapped turbomolecular pump (Balzer TPU50), (26) ion target.

differential pumping chamber (7) into the photodissociation chamber (4). The 3° angular spread of the beam corresponds to a beam width of 3 mm at the photodissociation region. The differential pumping chamber is evacuated by a liquid-nitrogen (LN₂) trapped 6 in. DP (Varian VHS6) with a pumping speed of ~2000 ℓ/s, while the photodissociation chamber is pumped by a freon-trapped 10 in. DP (Varian VHS10) having a pumping speed of ~5000 ℓ/s. The photodissociation chamber has two LN₂ cold traps, (5) and (11). When these cold traps are cooled to LN₂ temperature, the photodissociation chamber has a base pressure of ~1×10⁻⁸ Torr. During the experiment, the pressures in the differential and photodissociation chambers are maintained at ~1×10⁻⁵ and ≲8×10⁻⁸ Torr, respectively. When a pure CS₂ beam is used, the pressure in the photodissociation chamber is ≲2×10⁻⁸ Torr.

The nozzle is mounted on the rotatable beam source chamber (2) which is coupled to the molecular beam source chamber (8) using a bearing (9) and rotating "O"-ring seal assembly. The rotatable differential pumping chamber (6) is fabricated from a stainless-steel tube. One end of the rotatable differential pumping chamber is rigidly attached to and sealed against the rotatable molecular beam source chamber with an O ring, while the other end is opened to the differential pumping chamber. The seal between the rotatable differential pumping chamber and the photodissociation chamber is accomplished by a rotating O-ring seal as shown in the figure. A shaft (2a) secured to the center of the rotatable beam source chamber and placed along the common axis of the rotatable beam source and rotatable differential pumping chambers makes possible the rotation of the molecular beam in a plane perpendicular to the common axis. Since the rotatable beam source and rotatable differential pumping chambers rotate together as the shaft is turned, differential pumping for the molecular beam production is achieved without the rotation of any pumps. The rotation of the shaft outside the vacuum chamber can be made manually or automatically by a stepping motor.

The excimer laser used is either a Lambda Physik (MSC201) laser or a Questek (Model 2260) laser, which have a maximum repetition rate of 80 and 200 Hz at an output power of ~300 and 100 mJ at 193 nm, respectively. The output power of the Lambda Physik laser can be maintained at a constant value of 100 mJ operating at 80 Hz by a microprocessor (Lambda Physik ILC) for 3–4 h for one gas fill. The excimer laser beam has a cross section of ~8×24 mm².

The laser beam enters the differential pumping chamber through a MgF₂ focusing lens and traverses along the central axis of the rotatable differential pumping chamber before intersecting the CS₂ molecular beam at 90° at the photodissociation region. The fact that the CS₂ molecular beam is adjusted to intersect the common central axis of the rotatable beam source and the rotatable differential pumping chambers ensures the crossing of the laser and the CS₂ beams at all directions of the CS₂ beam.

The mass spectrometric detector has four stages of differential pumpings. The first (17) and second (18) differential pumping regions are evacuated by a turbomolecular

pump (Balzer TPU310) and an ion pump (Ultek 220 ℓ/s DI pump), respectively. The ionizer (20) is mounted inside the ionization chamber which is cooled to LN₂ temperature during the experiment. The ionizer is an axial ionizer (Extranuclear Model 041-1) which has an acceptance aperture of ~4.8 mm in diameter and a length of ~1 cm. The emission current of the ionizer used is <2.5 mA in this experiment. The ionization region (19) is pumped by a 120 ℓ/s ion pump (Ultek DI pump) and has a base pressure of ~5×10⁻¹¹ Torr. The apertures between the first and second differential and the ionization chambers are 6 mm in diameter. During this experiment, the pressures in the first and second differential and ionization regions are ≲1×10⁻⁸, ~5×10⁻¹⁰, and ~2×10⁻¹⁰ Torr, respectively. The quadrupole mass filter (QMF) is constructed of four stainless-steel rods which have a diameter of 1.9 cm and a length of 21 cm and are symmetrically held in a circle of 3.55 cm diameter. The ion detector is a Daly-type scintillation detector²⁹ which consists of an ion target (26) and a scintillator-photomultiplier assembly (24). The ion detector chamber is separated from the second differential pumping region by the QMF and a sheet metal wall. The vacuum in the ion detector chamber is maintained by a LN₂ trapped turbomolecular pump (Balzer TPU50).

The detector chamber (16) is mounted on a platform which is supported on a linearly movable rail assembly (not shown in the figure). Using the rail assembly, the distance between the photodissociation region and the ionizer can be varied continuously in the range of ~35–110 cm. The CS₂ molecular beam axis in the horizontal direction and the central axis of the ionizer define the detector axis. The positions of the platform and rail assembly are carefully adjusted such that the central axis of the ionizer remains in alignment with the detector axis as the detector chamber moves along the full range of rail. The laboratory angle (θ_{lab}) is the angle between the CS₂ molecular beam and the detector axis. The detector chamber is coupled to the photodissociation chamber with a flexible bellow (12) which serves to relieve the slight mechanical misalignment of the two chambers.

The detector and photodissociation chambers can be isolated by isolation valves (13). In order to change the distance between the photodissociation region and the ionizer, i.e., the flight path, an extension tube of the desired length can be placed between the valves. The isolation valves allow the replacement of the extension tube without venting the detector and photodissociation chambers.

In addition to the two apertures on the differential pumping walls in the detector, there are two more defining apertures along the detector axis. The first aperture (3 mm in diameter) is attached to the LN₂ cold trap (11) in the photodissociation chamber. The adjustable aperture (15), located between the extension tube and the isolation valve of the detector chamber, has an aperture of 6 mm in diameter in the normal photodissociation experiment. In the case when it is necessary to orient the CS₂ beam at the detector ($\theta_{\text{lab}} = 0^\circ$) such as in the experiment of measuring the velocity distribution of the CS₂ molecular beam, the adjustable aperture is reduced to a diameter of 0.127 mm.

The data acquisition and operation of the apparatus is

controlled by a LSI-11/23 minicomputer. The TOF spectrum is recorded on a homemade 1024 channel scaler which has a minimum channel width of 0.3 μ s. The multichannel scaler (MCS) is started by a trigger pulse signifying the firing of the laser. Time-of-flight spectra have also been recorded using a pulsed molecular beam valve (Newport Research Corp.). In a pulsed molecular beam experiment, the trigger pulse to the MCS and the excimer laser is delayed by $\sim 600 \mu$ s with respect to the trigger pulse for opening the pulsed valve.

In order to obtain the translational energy distribution from TOF spectra of photofragments, it is necessary to measure the velocity distribution of the CS₂ molecular beam. Two methods are used here to determine the velocity of CS₂ in this experiment. The first method involves using a TOF chopper wheel to chop the CS₂ beam and record the TOF spectrum of CS₂ from the wheel to the ionizer. In such an experiment, an aluminum chopper wheel with a diameter of 20 cm and two opening slots is placed between the photodissociation region and the first aperture along the detector. The two opening slots on the edge of the wheel are 0.2 mm wide and 5 mm deep and are separated by 180°. For a chopping frequency of 200 Hz, the chopper produces a CS₂ pulse of 1.6 μ s wide every 2.5 ms. The MCS is initiated by a trigger pulse from a photodiode which marks the production of the CS₂ pulse by the chopper wheel. The second method is the laser hole burning method. By firing the excimer laser at the CS₂ molecular beam, one finds that the intensity of the CS₂ beam along the detector axis is reduced for a time equal to the pulse width (15 ns) of the laser. The reduction of the CS₂ signal is due to the dissociation of CS₂ after the absorption of a 193 nm photon. The evolution of the laser burn hole from the photodissociation region to the ionizer recorded by the MCS gives an accurate measure of the velocity spread (Δv) and velocity (v) of the CS₂ molecular beam.

To find the flight time of a photofragment traveled from the photodissociation region to the ionizer, the time required for the ion to drift from the ionizer to the ion detector must be accounted for. The ion drift time through the QMF depends on the ion mass m and ion energy to the QMF. The ion drift time for several ions ($m/e = 2, 18, 32, 44,$ and 76) have been determined by applying a voltage pulse to the ion extraction lens of the ionizer and measuring the arrival times of the ions at the ion detector with respect to the triggered voltage pulse using an oscilloscope. As expected, at a given ion entrance energy to the QMF, the ion drift time is linearly proportional to \sqrt{m} . The actual flight time of the neutral CS₂ or photofragments is equal to the difference in time measured by the MCS and the ion drift time of the corresponding ion.

III. DATA ANALYSIS

The analysis of the TOF data involves the transformation of the laboratory TOF spectra into c.m. translational energy distributions. The transformation equation for laboratory to c.m. coordinates have been discussed in detail previously.^{30,31} The electron impact ionizer used here is a number density detector. The c.m. flux $I_{c.m.}(E_{c.m.}, \theta_{c.m.})$ at a given c.m. angle ($\theta_{c.m.}$) and a c.m. translational energy

($E_{c.m.}$) is related to the measured laboratory TOF signal $N_{lab}(t, \theta_{lab})$ and the corresponding θ_{lab} and arrival time t by the equation

$$I_{c.m.}(E_{c.m.}, \theta_{c.m.}) \propto t^3 u N_{lab}(t, \theta_{lab}), \quad (3)$$

where u is the c.m. velocity of the photofragment. The translational energy distributions presented here are obtained by the direct application of Eq. (3). The velocities for CS₂ are assumed to be equal to the most probable velocities (v_{mp}) measured by the chopper wheel method or laser hole burning technique. We have ignored the effect of the apparatus resolution factors on the observed TOF distributions.

IV. RESULTS

A. Velocity distributions of the CS₂ and (CS₂)₂ beams

Figures 2(a)–2(d) show the laser hole burning spectra of CS₂ observed in a pure CS₂ beam at $P_0 = 150$ Torr, a CS₂/Ne seeded beam at $P_0 = 517$ Torr, a CS₂/He seeded beam at $P_0 = 362$ Torr, and a CS₂/He seeded beam at $P_0 = 776$ Torr, respectively. The most probable velocities (v_{mp}) and the ratio $\Delta v/v_{mp}$ for the CS₂ beam determined by the spectra are summarized in Table I. Here, Δv represents the velocity spread (FWHM) of the CS₂ beam. In this experiment, the velocity spread of CS₂ is a major limitation to the resolution of the photofragment TOF measurements. The TOF spectrum of CS₂ from the pure CS₂ beam has also been measured by the chopper wheel method. The values of v_{mp} and $\Delta v/v_{mp}$ for the pure CS₂ beam obtained from the TOF spectrum of CS₂ are consistent with those determined from the laser hole burning spectrum shown in Fig. 2(a). Since the masses of the carrier gases are lighter than that of CS₂, the values of v_{mp} for CS₂ from the seeded beams are greater than that for the pure CS₂ beam. The $\Delta v/v_{mp}$ value for the CS₂/He seeded beam at $P_0 = 776$ Torr is ~ 2.5 times smaller than that for the pure CS₂ beam. Considerable amount of

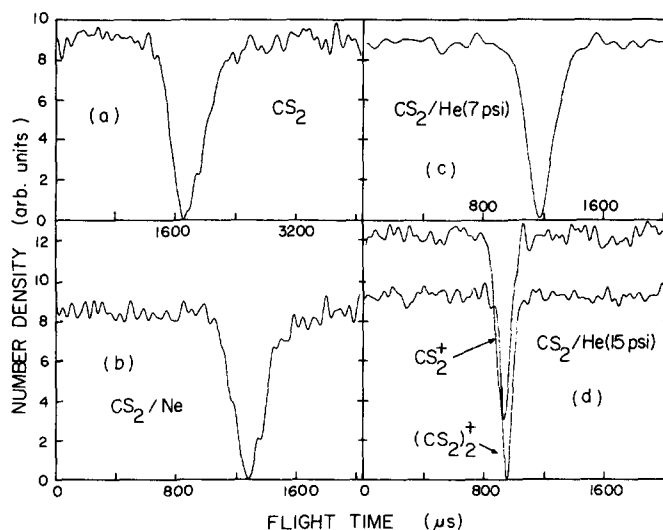


FIG. 2. Laser hole burning spectra for CS₂ in (a) a pure CS₂ beam ($P_0 = 150$ Torr), (b) a CS₂/Ne seeded beam ($P_0 = 517$ Torr), (c) a CS₂/He seeded beam (362 Torr), and (d) a CS₂/He seeded beam ($P_0 = 776$ Torr) (upper spectrum); (d) laser hole burning spectra for (CS₂)₂ in a CS₂/He seeded beam ($P_0 = 776$ Torr) (lower spectrum).

TABLE I. Characteristics of the CS₂ and (CS₂)₂ beams.

Nozzle conditions ^a	v_{mp} ^{b,d}	$\Delta v/v_{mp}$ ^{c,d}
Pure CS ₂ beam	$v_{mp}(\text{CS}_2) = 4.68 \times 10^4 \text{ cm/s}^e$	0.25 ^e
$P_0 = 150 \text{ Torr}, T_0 = 300 \text{ K}$		
CS ₂ /Ne seeded beam	$v_{mp}(\text{CS}_2) = 6.68 \times 10^4 \text{ cm/s}$	0.15
$P_0 = 517 \text{ Torr}, T_0 = 300 \text{ K}$		
CS ₂ /He seeded beam	$v_{mp}(\text{CS}_2) = 7.42 \times 10^4 \text{ cm/s}$	0.15
$P_0 = 362 \text{ Torr}, T_0 = 300 \text{ K}$		
CS ₂ /He seeded beam	$v_{mp}(\text{CS}_2) = 9.36 \times 10^4 \text{ cm/s}$	0.10
$P_0 = 776 \text{ Torr}, T_0 = 300 \text{ K}$	$v_{mp}[(\text{CS}_2)_2] = 9.09 \times 10^4 \text{ cm/s}$	0.08

^aNozzle diameter = 0.127 mm.

^bMost probable velocity.

^c Δv represents the velocity spread (FWHM).

^dValues measured using the laser hole burning method, $L = 84.5 \text{ cm}$.

^eValues of $\Delta v_{mp}/v_{mp}$ determined from the laser hole burning spectrum and the TOF chopper wheel method are in agreement.

CS₂ dimer and clusters are formed in the CS₂/He seeded beam at $P_0 = 776 \text{ Torr}$. The laser hole burning spectrum for (CS₂)₂ formed in the CS₂/He seeded beam at $P_0 = 776 \text{ Torr}$ is depicted in the lower panel of Fig. 2(d). Due to the slippage effect in the seeded supersonic beam, the velocity of (CS₂)₂ is slightly lower than that of CS₂. The $\Delta v/v_{mp}$ value for (CS₂)₂ is found to be smaller than that for CS₂. The shoulder observed at the longer flight time side of the CS₂⁺ dip is probably contributed by CS₂ dimer and higher CS₂ clusters. It is likely that the contribution to the CS₂⁺ dip from CS₂ dimer and clusters has broadened the CS₂⁺ dip. We believe that the $\Delta v/v_{mp}$ values for CS₂ are upper bounds.

B. Effect of ionizer conditions on TOF measurements

In the TOF measurements of neutral photofragments such as this experiment, the neutral photofragments are ionized in the ionizer before mass filtering and detection. We find that the conditions of the ionizer can affect significantly the appearance of the TOF spectrum of a photofragment. Figures 3(a) and 3(b) compare the TOF spectra of S from CS₂ recorded at two ion extraction voltages of ~ 8 and 0 V, respectively. The ion extraction voltage is the difference in voltage applied to the grid cage where the ions are formed and the ion extraction lens next to the cage. To extract ions from the cage, the potential of the ion extraction lens is lower than the cage. Other than the ion extraction voltage, these two spectra are recorded at the same experimental conditions. The spectrum in Fig. 3(a) exhibits two steplike structures and a sharp peak, whereas the spectrum in Fig. 3(b) only reveals a single broad peak. Furthermore, the first onset of the spectrum in Fig. 3(b) is delayed by $\sim 80 \mu\text{s}$ compared to that of the spectrum in Fig. 3(a). We believe that the delay of the TOF of S observed in Fig. 3(b) is due to the space charge effect in the ionizer at 0 V ion extraction voltage. Under this condition the S⁺ ion trapped by the space charge potential in the ionizer may be responsible for washing out the TOF structure of the neutral photofragment. A similar observation is found in the comparison of the TOF spectrum of CS obtained using ion extraction voltages of 0 and 8 V. The comparison of TOF spectra recorded at different ion extraction voltages suggests that it is important to minimize

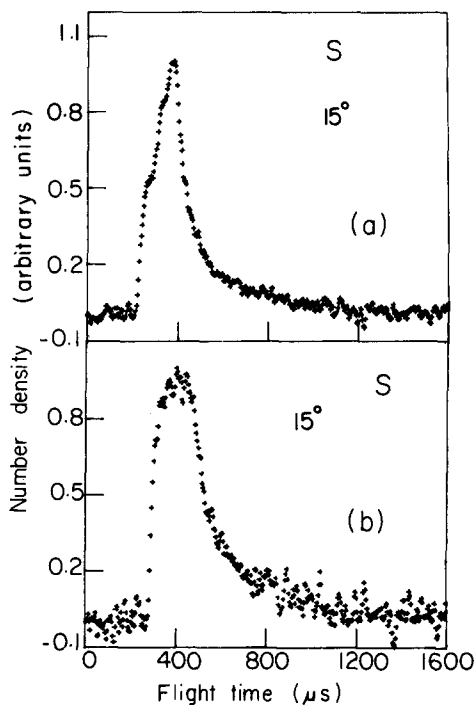


FIG. 3. TOF spectra for S obtained using an ion extraction voltage of (a) 8 V, (b) 0 V with respect to the ionizer cage [$L = 52.7 \text{ cm}$, $\theta_{lab} = 15^\circ$, $P_0 = 150 \text{ Torr}$ (pure CS₂), $T_0 = 298 \text{ K}$, electron energy = 50 eV, laser power = 20–120 mJ].

the effect of the space charge potential minimum in the ionizer by applying a sufficiently high ion extraction voltage when performing TOF measurements. All TOF spectra presented in this report were obtained with an ion extraction voltage $\sim 8 \text{ V}$.

C. Effects of electron energy and laser power on TOF measurements

From energetic consideration, CS(X, v) can be produced in $v = 0-13$ and $v = 0-5$ by reactions (1) and (2), respectively. In the TOF measurements of S and CS, it is important to examine the effects of the ionization reactions



on the TOF spectra. If processes (3) and (4) depend on v and/or the cross section for process (5) is high, the measured TOF spectra of CS and S would be erroneous. To minimize the extent of process (5), we have used an ionization electron energy of 50 eV in this experiment. Since the yield of S⁺ from CS(X, v) is expected to depend on the ionization electron energy, it is possible to estimate the effect of process (5) by comparing the TOF spectra of S and CS measured at different electron energies. Figures 4(a) and 4(b) depicted the TOF spectra of CS and S recorded at $\theta_{lab} = 10^\circ$ and an electron energy of 50 eV, respectively. The two spectra have similar structure except that the spectrum of CS is shifted toward longer arrival time compared to the S spectrum. Taking into account the counting statistics, the S spectrum measured at an electron energy of 50 eV is in agreement with that obtained at an electron energy of 20 eV [Fig. 4(c)]. This

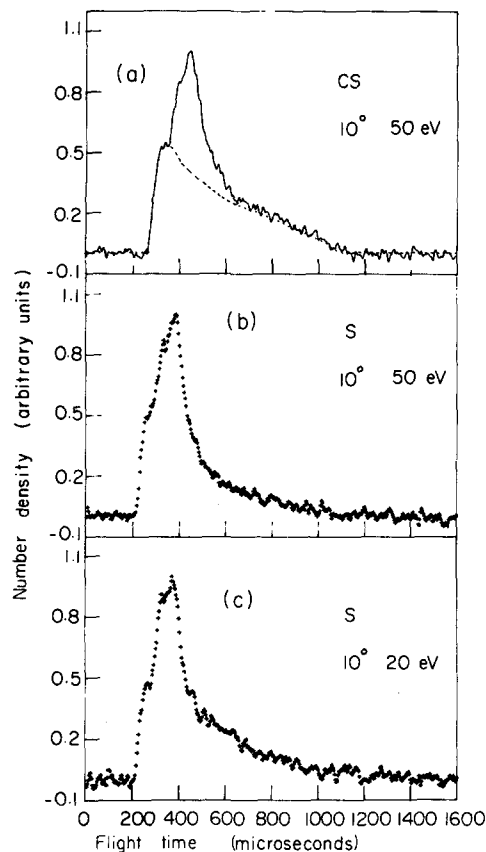


FIG. 4. (a) TOF spectrum of CS observed using an electron energy of 50 eV; (b) TOF spectrum of S observed using an electron energy of 50 eV; (c) TOF spectrum of S observed using an electron energy of 20 eV [$P_0 = 150$ Torr (pure CS₂), $T_0 = 298$ K, $L = 52.7$ cm, $\theta_{\text{lab}} = 10^\circ$, laser power = 20–120 mJ].

observation leads us to conclude that process (5) at the electron energy of 50 eV has little effect on the TOF measurements. We arrive at the same conclusion in the comparison of the TOF spectra of CS measured at electron energies of 20 and 50 eV.

The translational energy distributions derived from the TOF spectra of CS and S at $\theta_{\text{lab}} = 10^\circ$ and an electron energy of 50 eV are compared in Fig. 5(a). The two distributions have been normalized to one at the most probable translational energy of ~ 8 kcal/mol. Taking into account the experimental uncertainties of both spectra, the translational energy distributions are in agreement, indicating that process (4) only depends weakly on ν and has little effect on the measured TOF spectra.

Time-of-flight spectra of S and CS have been recorded at different laser powers ranging from ~ 20 to 150 mJ. The laser power is found to have no discernible effect on the TOF spectra of S and CS. This observation shows that the further decomposition of CS($X, \nu > 5$) by absorbing a second excimer photon within the photodissociating laser pulse is insignificant under the present experimental conditions. A similar conclusion was reached in the recent laser kinetic spectroscopic study of Kanamori and Hirota.²¹ The majority of TOF spectra reported here are recorded using a constant laser power of 100 mJ.

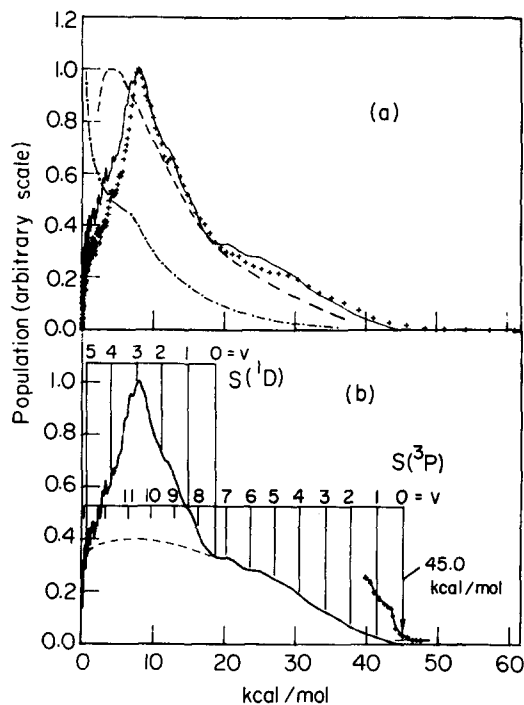


FIG. 5. (a) Translational energy distributions: — derived from TOF spectrum of CS [see Fig. 4(a)]; + + + derived from TOF spectrum of S [see Fig. 4(b)]; --- Ref. 18; - - - Ref. 20. (b) Correlation of the translational energy distribution with the expected translational energies for the formation of CS($X, \nu = 0-5$) + S(1D) and CS($X, \nu = 0-13$) + S(3P).

D. TOF spectra of photofragments from CS₂/He(Ne) seeded beams

The TOF spectra of S obtained at $\theta_{\text{lab}} = 7, 15, 30, 45, 60$, and 75° using the CS₂/He seeded beam at $P_0 = 776$ Torr are plotted in Figs. 6(a)–6(f), respectively. The TOF spectra of CS are found to be consistent with the S spectra. Since the ion background in the QMF for mass 32 is lower compared to that for mass 44 and a better signal to noise can be obtained at a given accumulation time for the S spectrum than CS spectrum, we only show the TOF spectra of S here. Figures 7(a) and 7(b) depicted the S spectrum recorded at $\theta_{\text{lab}} = 7^\circ$ and 15° using the seeded CS₂/Ne beam at $P_0 = 517$ Torr and CS₂/He beam at 362 Torr, respectively. The TOF spectrum of S obtained at $\theta_{\text{lab}} = 30^\circ$ using the pulsed CS₂/He seeded beam at $P_0 = 1034$ Torr is plotted in Fig. 7(c). We found that a signal-to-noise improvement of ~ 100 was achieved by using a pulsed CS₂/He beam in comparison with that obtained with a continuous pure CS₂ beam at $P_0 = 150$ Torr.

The translational energy distributions derived from the TOF spectra of S at $\theta_{\text{lab}} = 30^\circ, 45^\circ, 60^\circ$, and 75° [Figs. 6(c)–6(f)] are shown in Figs. 8(c)–8(f), while the translational energy distributions obtained from the spectra in Figs. 7(a) and 7(b) are shown in Figs. 6(a) and 6(b), respectively.

When the seeded CS₂/He(Ne) beams are used, photofragments from CS₂ dimer and clusters are also observed at small θ_{lab} ($\lesssim 20^\circ$). The TOF spectra for S₂⁺ observed at $\theta_{\text{lab}} = 7^\circ$ and 15° using the seeded CS₂/He beam at $P_0 \approx 776$ Torr are depicted in Figs. 9(a) and 9(b), respectively. The TOF spectra for the (CS₂)₂⁺, C₂S₂⁺, and CS₃⁺ ions are shown in

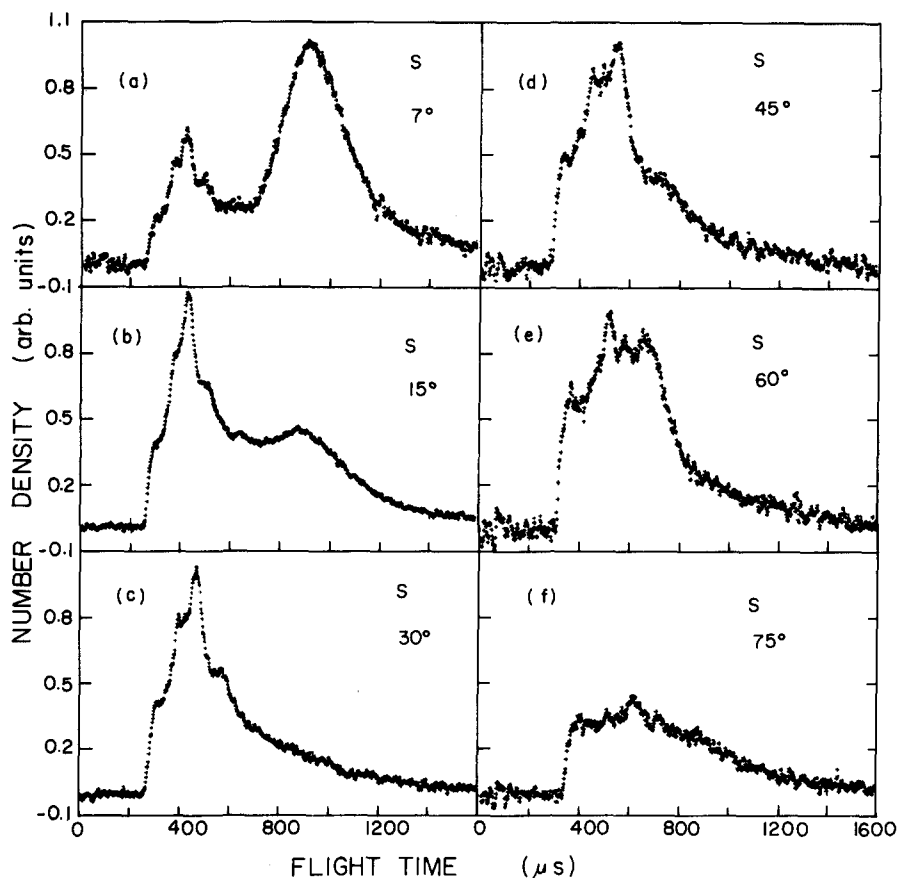


FIG. 6. TOF spectra of S observed at (a) $\theta_{\text{lab}} = 7^\circ$; (b) 15° ; (c) 30° ; (d) 45° ; (e) 60° ; and (f) 75° ($L = 84.5$ cm, CS₂/He seeded beam at $P_0 = 776$ Torr).

Figs. 10(a)–10(c), respectively. No efforts were made to measure TOF spectra for ions heavier than (CS₂)₂⁺.

V. DISCUSSION

Based on the conservation of energy, we have the relation

$$h\nu + E_{\text{int}} = D_0(\text{SC} - \text{S}) + E_e + E_v + E_r + E_{\text{c.m.}}, \quad (6)$$

where $h\nu$ is the photodissociation energy, E_{int} is the initial internal energy of the parent CS₂ molecule, which is assumed to be negligible due to the cooling effect in a supersonic beam, $D_0(\text{SC} - \text{S})$ is the SC–S bond dissociation energy, and E_e , E_v , and E_r are the electronic, vibrational, and rotational energy of the photofragments, respectively. The energy separation of the S(¹D₂) and S(³P₂) states is known to be 26.4 kcal/mol.² From the threshold energy for A→X emission of CS formed in the irradiation of CS₂ with VUV light, Okabe¹¹ has determined an upper bound of 102.9 ± 0.32 kcal/mol for $D_0(\text{SC} - \text{S})$. This value is found to be in excellent agreement with the value of 102.7 ± 0.7 kcal/mol obtained from the photoionization experiment.³² The vibrational spacings of CS(X) have been reported previously.³³ The Newton diagram for the formation of S(¹D) and S(³P) by 193 nm photodissociation of the pure CS₂ beam at $P_0 = 150$ Torr, constructed using Eq. (6), is depicted in Fig. 11. The two dashed circles show the expected maximum velocities of the S fragments produced by reactions

(1) and (2). The magnitudes of the velocities for S(³P) with CS(X) in $v = 0$ –13 and S(¹D) with CS(X) in $v = 0$ –5 are also shown in the figure. The velocities for S are calculated by assuming $E_r = 0$. The values for θ_{lab} shown are where data were taken. The signal for S was found to decrease rapidly as θ_{lab} is increased (see Fig. 12).

It is clear from the Newton diagram that when the S fragment is detected at large θ_{lab} , e.g., $\theta_{\text{lab}} = 90^\circ$, slow S fragments with velocities less than the CS₂ beam velocity cannot reach the detector. The primary motivation of the coaxial TOF experiment of McCrary *et al.*²⁰ is to detect photofragments at all translational energies. They concluded from their coaxial TOF measurement that a considerable fraction of photofragments are formed at low translational energies and these slow photofragments were not observed in the perpendicular TOF measurement of Yang *et al.*¹⁸ Figure 5(a) compares the translational energy distributions obtained by McCrary *et al.*, Yang *et al.*, and this work. The translational energy distribution of this work is derived from the CS spectrum shown in Fig. 4(a), which is measured at $\theta_{\text{lab}} = 10^\circ$. The peaks of the distributions are arbitrarily normalized to one. The results of Yang *et al.* and this work are in qualitative agreement except that the peak of their distribution is lower by ~ 3 kcal/mol compared to that of ours. The nearly exponential increase in population towards low translational energy found by McCrary *et al.* is not confirmed in this experiment. However, the translational energy distribution de-

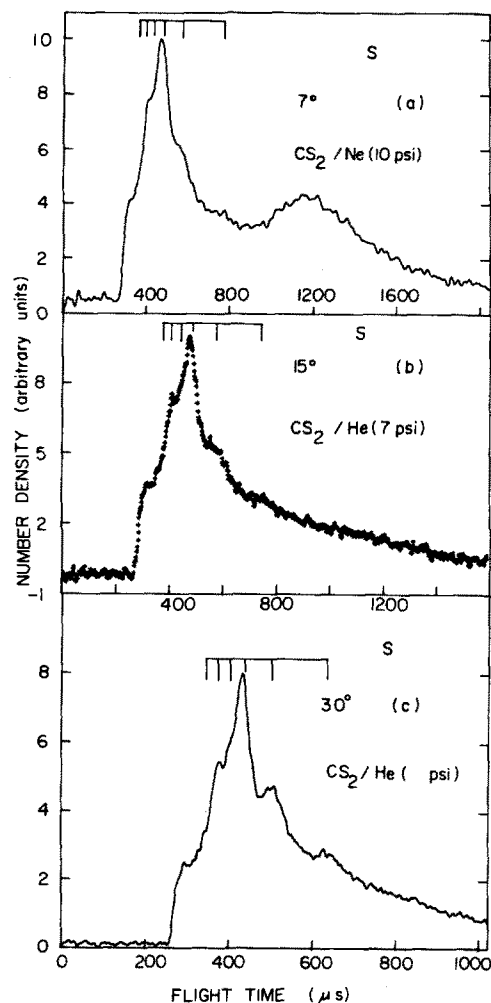


FIG. 7. TOF spectra of S. (a) $\theta_{\text{lab}} = 7^\circ$, CS₂/Ne seeded beam at $P_0 = 517$ Torr; (b) $\theta_{\text{lab}} = 15^\circ$, CS₂/He seeded beam at $P_0 = 357$ Torr; and (c) $\theta_{\text{lab}} = 30^\circ$, pulsed CS₂/He seeded beam at $P_0 = 1034$ Torr, pulse rate = 48 Hz ($L = 84.5$ cm).

rived from their TOF spectrum of CS measured at $\theta_{\text{lab}} = 90^\circ$, which is not shown in the figure, is consistent with our results. When the neutral CS₂ beam is aimed directly at the ionizer, i.e., $\theta_{\text{lab}} = 0^\circ$, the ion background for CS⁺ is expected to be very high. The coaxial TOF spectrum of CS recorded by McCrary *et al.* might have been affected by the space charge effect in the ionizer.

The relative populations of the spin-orbit sublevels of S(³P_J) were determined to be ³P₂:³P₁:³P₀ = 4.0:2.1:1.0 in the VUV laser induced fluorescence experiment of Waller *et al.*²² The positions in translational energy correlating to the formation of CS(*X*, $\nu = 0-5$) + S(¹D₂) and CS(*X*, $\nu = 0-13$) + S(³P₂) are indicated in Fig. 5(b). The threshold for the formation of CS(*X*, $\nu = 0$) + S(³P₂) is found to be 45.0 ± 0.4 kcal/mol in this experiment. Assuming $E_{\text{int}} = 0$, we calculate a value of 102.9 ± 0.4 kcal/mol for $D_0(\text{SC} - \text{S})$ which is in excellent agreement with those determined previously in the fluorescence¹¹ and photoionization³² experiments. The uncertainties of ± 0.4 kcal/mol are in accordance with the variation of the threshold values observed in the translational energy distributions shown in Figs. 8(a)–8(f) which are derived from the TOF spectra of S measured using the seeded CS₂/He(Ne) beam method. At

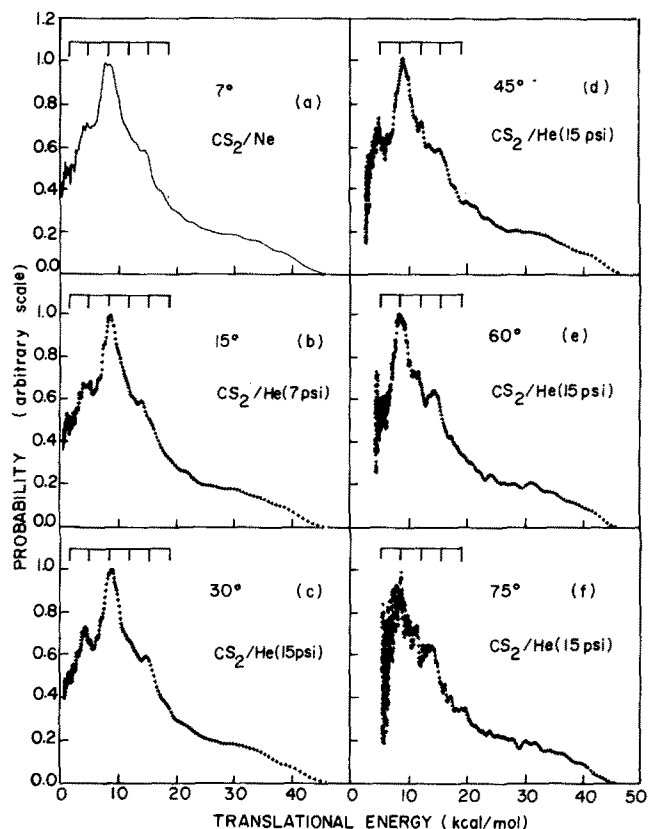


FIG. 8. Translational energy distributions derived from TOF spectra of S measured at (a) $\theta_{\text{lab}} = 7^\circ$, CS₂/Ne seeded beam at $P_0 = 517$ Torr, (b) $\theta_{\text{lab}} = 15^\circ$, CS₂/He seeded beam at $P_0 = 357$ Torr, (c) $\theta_{\text{lab}} = 30^\circ$, CS₂/He seeded beam at $P_0 = 776$ Torr, (d) $\theta_{\text{lab}} = 45^\circ$, CS₂/He seeded beam at $P_0 = 776$ Torr, (e) $\theta_{\text{lab}} = 60^\circ$, CS₂/He seeded beam at $P_0 = 776$ Torr, and (f) $\theta_{\text{lab}} = 75^\circ$, CS₂/He seeded beam at $P_0 = 776$ Torr.

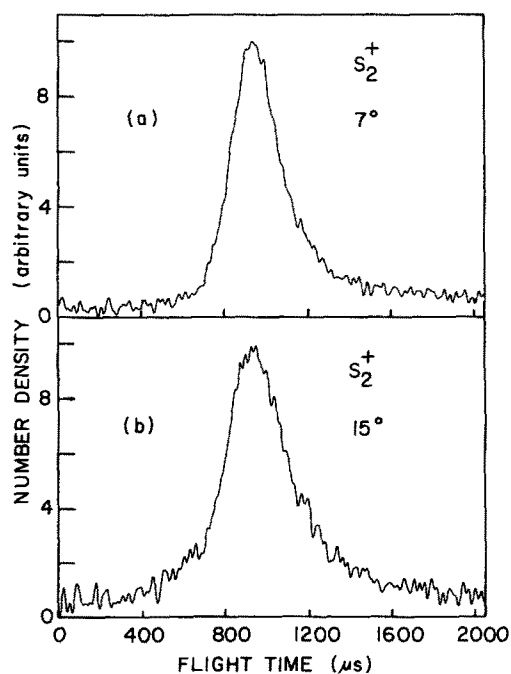


FIG. 9. TOF spectra for S₂⁺ observed at (a) $\theta_{\text{lab}} = 7^\circ$ and (b) $\theta_{\text{lab}} = 15^\circ$ ($L = 84.5$ cm, CS₂/He seeded beam at $P_0 = 776$ Torr).

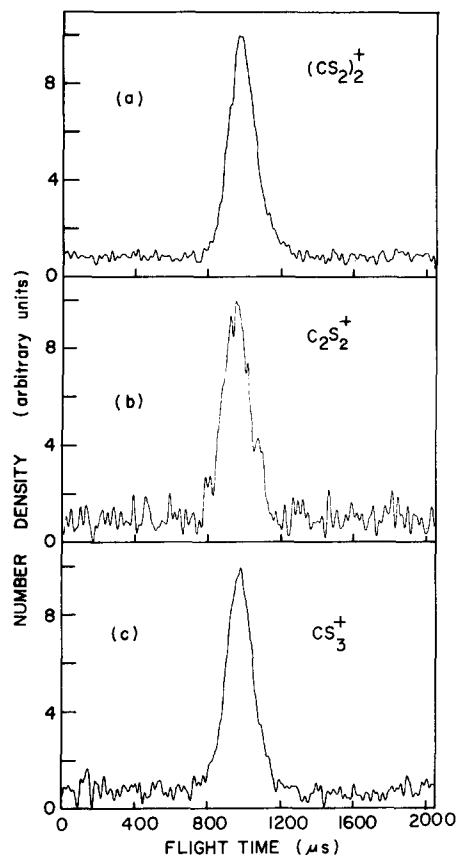


FIG. 10. TOF spectra for (a) $(CS_2)_2^+$, (b) $C_2S_2^+$, and (c) CS_3^+ observed at $\theta_{lab} = 7^\circ$ ($L = 84.5$ cm, CS_2/He seeded beam at $P_0 = 776$ Torr).

18.7 kcal/mol, there is a clear break in the translational energy distribution which coincides with the thermochemical threshold for the formation of $CS(X, v = 0) + S(^1D_2)$. This break was observed, but less clear, in the translational energy distribution reported by Yang *et al.*

Because of the narrower velocity spreads for parent CS_2 achieved in the $CS_2/He(Ne)$ seeded beams compared to that in the pure CS_2 beam, the resolutions of the TOF spectra

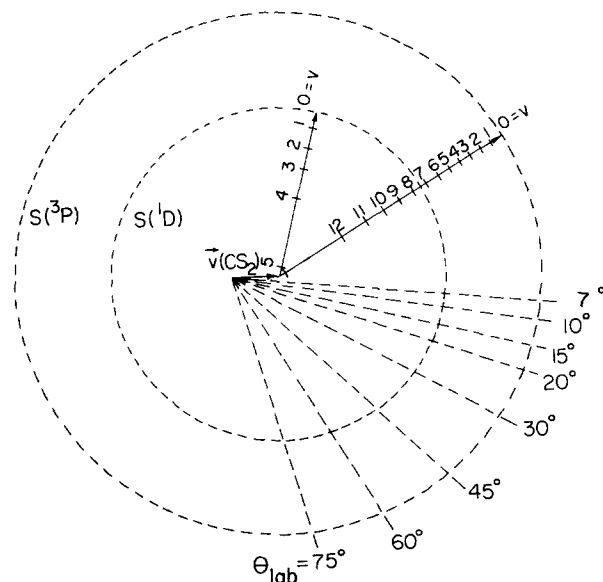


FIG. 11. Kinematics for the 193 nm photodissociation of a pure CS_2 beam.

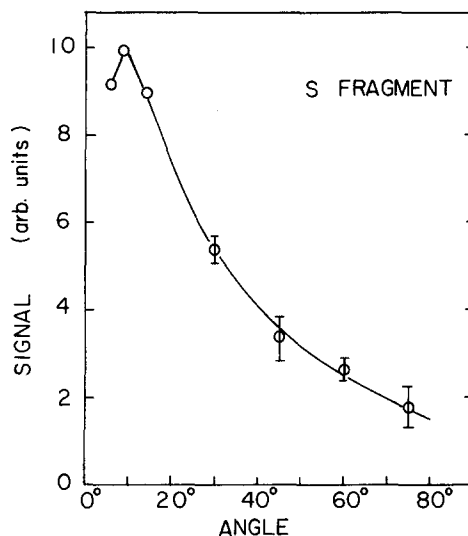


FIG. 12. Laboratory angular distribution of S.

recorded using the seeded $CS_2/He(Ne)$ beams are higher than that of the spectra shown in Figs. 4(a) and 4(b). Structures which can be correlated with the formation of $CS(X, v = 0-5) + S(^1D_2)$ are discernible in the TOF spectra of S [Figs. 6(a)–6(f) and Figs. 7(a)–7(c)] using seeded $CS_2/He(Ne)$ beams. The stick marks in Figs. 7(a)–7(c) and Figs. 8(a)–8(f) indicate the expected flight times and translational energies, respectively, for the formation of $CS(X, v = 0-5) + S(^1D_2)$. The structures corresponding to $v = 4$ and 5 are most well-resolved in the TOF spectrum of S [Fig. 7(c)] measured using the pulsed CS_2/He seeded beam. The fragment laboratory velocity v_{lab} is equal to $u + v_{mp}$. As θ_{lab} increases, the magnitude of v_{lab} decreases. Thus, the TOF resolution improves as θ_{lab} increases. This effect can be seen in Figs. 8(a)–8(f). The broad peaks appearing at longer flight times in Figs. 6(a), 6(b), and 7(a) are due to the photodissociation of CS_2 dimer and clusters and will be discussed in a later section. Although the TOF spectra of S observed at $\theta_{lab} = 45^\circ, 60^\circ,$ and 75° are quite different from those at $\theta_{lab} < 30^\circ$, the translational energy distributions derived from these spectra are essentially identical. The transformation of the slow broad peaks in the TOF spectra into energy space gives a low energy peak at translational energy well below 1 kcal/mol. The low energy peak originating from the slow broad peak in Fig. 7(a) has been deleted from the translational energy distribution of Fig. 8(a).

The absorption band of CS_2 in the region between 185–230 nm has been assigned as the linear \rightarrow bent, $X^1\Sigma_g^+ \rightarrow \tilde{A}^1B_2$, transition.^{34–36} The transition results in excitation of both the symmetric stretch and bending vibrations and gives rise to a complex absorption spectrum. The \tilde{A}^1B_2 state has a lifetime of ~ 1 ps and a very low fluorescence quantum yield ($< 10^{-3}$)^{18,37} The rapid predissociation of $CS_2(\tilde{A}^1B_2)$ is believed to be the mechanism for the formation of $CS + S$. The bent structure of $CS_2(\tilde{A}^1B_2)$ is consistent with the observation that $CS(X, v)$ fragments are produced in a broad distribution of rotational states.²¹ The lack of vibrational structure in the TOF spectra for the $CS(X, v) + S(^3P)$ channel can be attributed to the rotational excitation of $CS(X, v)$

and the population of S(³P) in the spin-orbit sublevels. Although CS(*X*,*v*) fragments associating with the S(¹D₂) channel were also found to be rotationally excited, the rotational excitation energy ranges for CS(*X*,*v*) formed in the singlet channel allowed by energy conservation are much narrower than those in the triplet channel. The TOF experiment of Yang *et al.* revealed an isotropic angular distribution of CS and estimated a lower limit of 0.6 ps for the predissociation lifetime of CS₂. However, the recent experiment of Waller *et al.* using Doppler spectroscopic techniques observed an anisotropy in dissociation and provided a lifetime of 2 ps for the excited \tilde{A}^1B_2 state. The discrepancy between the two experiments has been attributed to rotational cooling of CS₂ molecules by supersonic expansion in the experiment of Waller *et al.*, while a thermal CS₂ effusive beam was used in the work of Yang *et al.* The 193 nm excimer laser beam used in this experiment is not polarized. The CS and S fragments are expected to scatter isotropically in space. The finding that translational energy distributions [Figs. 8(a)–8(f)] derived from TOF spectra at different θ_{lab} are identical is consistent with this expectation.

The TOF measurement cannot provide a clear separation between the singlet and triplet channels. Thus, the S(³P)/S(¹D) ratio cannot be determined unambiguously from the translational energy distribution. Since the intensities of CS₂ dimers and clusters produced in the pure CS₂ beam are negligible compared to that of the CS₂ monomer, the TOF spectrum of CS shown in Fig. 4(a) is predominantly due to the dissociation of CS₂. The sharp rise in the CS spectrum at $\sim 354 \mu\text{s}$ which corresponds to the break at 18.7 kcal/mol in the translational energy distribution is assigned as the thermochemical threshold for reaction (2). Assuming the photodissociation products with translational energies below 18.7 kcal/mol are all formed in the singlet channel, we calculate a lower limit of 0.4 for the S(³P)/S(¹D) ratio. There seems to be a break at $\sim 650 \mu\text{s}$, midway at the drop-off of the TOF signal from the peak at $\sim 440 \mu\text{s}$. If one connects the breaks at 354 and 650 μs by the dashed line as shown in Fig. 4(a) and assumes the signals above and below the dashed line to be due to the singlet and triplet channels, respectively, an estimate of 2.6 is obtained for the S(³P)/S(¹D) ratio. The division of the populations for the two channels in the translational energy distribution can be seen in Fig. 4(b). Similar exercises based on the translational energy distributions, shown in Figs. 8(a)–8(c), give values between 2.5 to 2.7 for the ratio. The estimate of 2.6 for the S(³P)/S(¹D) ratio is in agreement with a value of 2.8 ± 0.3 determined by Waller *et al.* This observation can be taken as a support for the data analysis described above.

Assuming the data analysis to be correct, we have deduced a bimodal vibrational distribution for CS(*X*,*v* = 0–13) produced by reactions (1) and (2). Figure 13 compares this distribution and those obtained in previous studies. The relative populations for CS(*X*,*v* = 5) have been normalized to have the same value. The relative vibrational populations for CS(*X*,*v* = 1–5) have been measured earlier by Bulter *et al.*¹⁷ in a laser induced fluorescence experiment. They found that the CS(*X*,*v*) fragments are formed with a maximum population at *v* = 3. As shown in the figure, this finding is

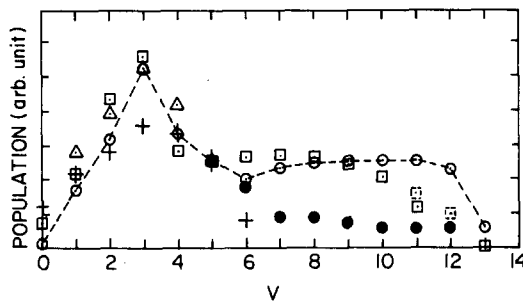


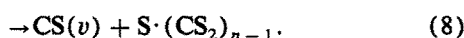
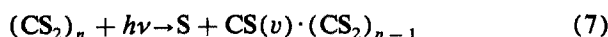
FIG. 13. Experimental values for the relative vibrational population of CS(*X*). ○: this work; □: Ref. 22; □·: values obtained using the translational energy distribution of Ref. 22 and the correct translational energies corresponding to the formation of CS(*X*,*v* = 11–13) (see text); △: Ref. 17; +: Ref. 18; ●: Ref. 20.

consistent with the conclusion of the later experiments.^{18,22} Taking into account the experimental uncertainties, the relative populations for CS(*X*,*v* = 0–5) measured by Bulter *et al.*, Waller *et al.*, and this work are in good agreement. Our results for *v* = 6–10 are also in accord with those obtained most recently by Waller *et al.* using Doppler spectroscopic techniques. The relative populations for CS(*X*,*v* = 11–12) estimated in this study are higher than those of Waller *et al.* As shown in Fig. 5(a), the populations of fragments at translational energies below ~ 8 kcal/mol derived from the TOF spectrum of S [Fig. 4(b)] are lower than those from the CS spectrum by $\sim 10\%$ – 20% . Therefore, it is possible that our values for *v* = 11–13 are $\sim 10\%$ – 20% too high. We note that the values for the translational energies of fragments corresponding to the formation of CS(*X*,*v* = 11–12) used by Waller *et al.* to determine the relative vibrational populations for *v* = 11–12 are incorrect. Using the correct translational energies for *v* = 11–13, together with their translational energy distribution, we obtained higher values for the populations of CS(*X*,*v* = 11–13) which are included in Fig. 13. The above considerations bring the results for *v* = 11–13 of the two experiments in satisfactory agreement. The relative populations for *v* = 7–12 measured by McCrary *et al.* seem to be too low.

The formation of C + S₂ from CS₂ requires 7.5 eV. (Ref. 38). Thus, S₂ cannot be produced by one photon absorption at 193 nm. Signals observed at ion masses corresponding to S₂⁺, (CS₂)₂⁺, C₂S₂⁺, and CS₃⁺ necessarily originate from photofragments of CS₂ dimers and clusters. All the TOF spectra of these ions are peaked at 930–970 μs (see Figs. 9 and 10). The slight variations in position of the peaks can be mostly accounted for by the different drift times of the ions from the ionizer to the ion detector. The slower broad peak resolved in the TOF spectrum of S at $\theta_{\text{lab}} = 7^\circ$ [Fig. 6(a)] has the maximum at the same position in flight time ($\sim 930 \mu\text{s}$), indicating that it is also produced by photofragments of CS₂ dimers and clusters. As mentioned above, a similar broad peak was found in the TOF spectrum of CS at $\theta_{\text{lab}} = 7^\circ$ which is not shown here. The heights of the slower broad peaks relative to the fast peaks in the S and CS spectra reduce substantially as *P*₀ is decreased. This is the most convincing evidence that the slower broad peak is due to CS₂ dimers and clusters. The magnitude of the slow broad peak diminishes

quickly as θ_{lab} is increased. At $\theta_{\text{lab}} = 30^\circ$, the broad peak is indiscernible in the S and CS spectra [see Fig. 6(c)]. The TOF peaks attributed to cluster fragmentation appear at essentially the same flight time position (925–950 μs) of the CS₂ beam, i.e., the cluster photofragments have nearly the same velocities as the parent CS₂ dimers and clusters and are strongly focused in the forward direction. This is the expected kinematic situation when the heavy fragment is detected in a light-heavy dissociation process.

The widths (FWHM) of the S₂⁺ TOF peak and the slower broad peaks in the S and CS spectra are identical and have a value of $\sim 260 \mu\text{s}$. The TOF peaks for (CS₂)₂⁺, C₂S₂⁺, and CS₃⁺ are also found to have the same width ($\sim 170 \mu\text{s}$) which is closer to the width ($\sim 104 \mu\text{s}$) of the CS₂ parent beam. The width of the TOF peak for an ion is a measure of the translational energy spread of the neutral photofragment from which the ion is produced. No attempt was made to characterize the distribution of CS₂ clusters in the experiment. According to the previous molecular beam photoionization study of CS₂ (Ref. 39), CS₂ clusters (CS₂)_n, $n = 2-5$, are formed with appreciable concentrations in the supersonic expansion of a CS₂/Ar seeded beam at $P_0 \approx 450$ Torr. Using a CS₂/He seeded beam at $P_0 = 776$ Torr, we expected that higher CS₂ clusters, $n > 5$ are produced. To a first approximation, one may consider the photodissociation of a CS₂ cluster as involving only one CS₂ molecule of the cluster



This approximation implies that the photodissociation cross section is linearly proportional to n . Thus the cluster photofragmentation can be dominated by those from higher clusters even though the dimer has the highest concentration in a supersonic expansion. Since the binding energies for CS(v) · (CS₂)_{n-1} and S · (CS₂)_{n-1} are weak, the further dissociation of these fragments are possible. For $v \geq 1$, vibrational predissociation of CS(v) · (CS₂)_{n-1} can be a highly efficient process. It is most likely that the TOF spectra for (CS₂)₂⁺, C₂S₂⁺, and CS₃⁺ are due to the heavier fragments of reactions (7) and (8). The reaction



is nearly thermal neutral.³⁹ The half reaction



is a feasible process. The lighter fragments, S, CS, and S₂ formed in reactions (7), (8), and (10), respectively, may account for the greater widths of the S, CS, and S₂ TOF peaks in comparison with those of the (CS₂)₂, C₂S₂⁺, and CS₃⁺ TOF peaks. Undoubtedly, the S⁺, CS⁺, and S₂⁺ signals also have contributions from heavier photofragments.

VI. SUMMARY

Higher resolution TOF spectra for CS and S from 193 nm photodissociation of CS₂ have been recorded using a crossed laser and molecular beam photofragmentation apparatus. The thermochemical thresholds for the formation of CS(X) + S(¹D₂) and CS(X) + S(³P₂) are determined to be

18.7 and 45.0 ± 0.4 kcal/mol, respectively, in excellent agreement with literature values. Using the translational energy distribution derived from the TOF data and the data analysis procedures described in the text, we estimate a value of 2.5 for the branching ratio S(³P)/S(¹D) which is consistent with the value determined most recently by Waller *et al.* using the VUV laser induced fluorescence method. The vibrational distribution for CS($X, v = 0-13$) measured in this study is also in satisfactory accord with the results of the latter experiment. Photofragments from CS₂ clusters are found to appear at small laboratory angles ($\theta_{\text{lab}} \lesssim 20^\circ$) with narrow energy spreads.

ACKNOWLEDGMENTS

C. Y. N. thanks Dr. I. M. Waller and Professor J. W. Hepburn for helpful discussions and Dr. A. M. Wodtke for providing us an unpublished time-of-flight spectrum of CS.

- ¹M. N. R. Ashfold, M. T. Macpherson, and J. P. Simons, *Top. Curr. Chem.* **86**, 1 (1979).
- ²H. Okabe, *Photochemistry of Small Molecules* (Wiley, New York, 1978).
- ³R. Bersohn, *J. Phys. Chem.* **88**, 5145 (1984), and references therein.
- ⁴S. R. Leone, *Adv. Chem. Phys.* **51**, 255 (1982).
- ⁵M. N. R. Ashfold, *Photophysics and Photochemistry in the Vacuum Ultraviolet*, edited by S. P. McGlynn *et al.* (Reidel, Boston, 1985), p. 409.
- ⁶G. G. Balint-Kurti and M. Shapiro, *Chem. Phys.* **61**, 137 (1981).
- ⁷R. G. W. Norrish and G. Porter, *Proc. R. Soc. London Ser. A* **200**, 284 (1950).
- ⁸F. J. Wright, *J. Phys. Chem.* **64**, 1648 (1960).
- ⁹A. B. Callear, *Proc. R. Soc. London Ser. A* **276**, 401 (1963).
- ¹⁰M. deSorgo, A. J. Yarwood, O. P. Strausz, and H. E. Gunning, *Can. J. Chem.* **43**, 1886 (1965).
- ¹¹H. Okabe, *J. Chem. Phys.* **56**, 4381 (1972).
- ¹²L. C. Lee and D. L. Judge, *J. Chem. Phys.* **63**, 2782 (1975).
- ¹³M. C. Addison, C. D. Byrne, and R. J. Donovan, *Chem. Phys. Lett.* **64**, 57 (1979).
- ¹⁴M. C. Addison, R. J. Donovan, and C. Fotakis, *Chem. Phys. Lett.* **74**, 58 (1980).
- ¹⁵T. R. Loree, J. H. Clark, K. B. Butterfield, J. L. Lyman, and R. Engleman, Jr., *J. Photochem.* **10**, 359 (1979).
- ¹⁶G. Dornhöfer, W. Hack, and W. Langel, *J. Phys. Chem.* **88**, 3060 (1984).
- ¹⁷J. B. Butler, W. S. Drozdowski, and J. R. McDonald, *Chem. Phys.* **50**, 413 (1980).
- ¹⁸S. Yang, A. Freedman, M. Kawasaki, and R. Bersohn, *J. Chem. Phys.* **72**, 4048 (1980).
- ¹⁹T. Ebata, M. Kawasaki, K. Obi, and I. Tanaka, *Bull. Chem. Soc. Jpn.* **52**, 3226 (1979).
- ²⁰V. R. McCrary, R. Lu, D. Zakheim, J. A. Russell, J. B. Halpern, and W. M. Jackson, *J. Chem. Phys.* **83**, 3481 (1985).
- ²¹H. Kanamori and E. Hirota, *J. Chem. Phys.* **86**, 3901 (1987).
- ²²I. M. Waller and J. W. Hepburn, *J. Chem. Phys.* **87**, 3261 (1987).
- ²³G. E. Busch, J. F. Corneliuss, R. T. Mahoney, R. I. Morse, D. W. Schlosser, and K. R. Wilson, *Rev. Sci. Instrum.* **41**, 1066 (1970).
- ²⁴G. E. Busch and K. R. Wilson, *J. Chem. Phys.* **56**, 3626 (1972); **56**, 3638 (1972); **56**, 3655 (1972).
- ²⁵R. K. Sander and K. R. Wilson, *J. Chem. Phys.* **63**, 4242 (1975).
- ²⁶R. J. Oldman, R. K. Sander, and K. R. Wilson, *J. Chem. Phys.* **63**, 4252 (1975).

- ²⁷R. D. Clear, S. J. Riley, and K. R. Wilson, *J. Chem. Phys.* **63**, 1340 (1975).
- ²⁸A. M. Wodtke and Y. T. Lee, *J. Phys. Chem.* **89**, 4744 (1985).
- ²⁹N. R. Daly, *Rev. Sci. Instrum.* **31**, 264 (1960).
- ³⁰T. T. Warnock and R. B. Bernstein *J. Chem. Phys.* **49** 1878 (1968).
- ³¹G. L. Catchen, J. Husain, and R. N. Zare, *J. Chem. Phys.* **69**, 1737 (1968).
- ³²V. H. Dibeler and J. A. Walker, *J. Opt. Soc. Am.* **57**, 1007 (1967).
- ³³T. Bergeman and D. Cossart, *J. Mol. Spectrosc.* **87**, 119 (1981).
- ³⁴A. E. Douglas and J. Zanon, *Can. J. Phys.* **42**, 627 (1964).
- ³⁵J. W. Rabalais, J. R. McDonald, V. Scherr, and S. P. McGlynn, *Chem. Rev.* **71**, 73 (1971).
- ³⁶R. J. Hemley, D. G. Leopold, J. L. Roebber, and V. Vaida, *J. Chem. Phys.* **79**, 5219 (1983).
- ³⁷K. Hara and D. Phillips, *J. Chem. Soc. Faraday Trans. 2* **74**, 1441 (1978).
- ³⁸D. R. Stull and H. Prophet, *Natl. Stand. Rev. Data Ser., Natl. Bur. Stand.* **37** (U.S. GPO Washington, D.C., 1971).
- ³⁹Y. Ono, S. H. Linn, H. F. Prest, M. E. Gress, and C. Y. Ng, *J. Chem. Phys.* **73**, 2523 (1980).